SCIENCE CHINA
Earth Sciences

•RESEARCH PAPER•

August 2022 Vol.65 No.8: 1510–1521
https://doi.org/10.1007/s11430-022-9948-6

High-precision potassium isotope analysis using the Nu Sapphire collision cell (CC)-MC-ICP-MS

Wenjun LI[1*], Mengmeng CUI[1,2], Qiqi PAN[2,3], Jing WANG[1], Bingyu GAO[1], Shanke LIU[1], Meng YUAN[2,3], Benxun SU[1,2†], Ye ZHAO[4], Fang-Zhen TENG[5] & Guilin HAN[6]

[1] *Key Laboratory of Mineral Resources, Institute of Geology and Geophysics, Chinese Academy of Sciences, Beijing 100029, China;*
[2] *University of Chinese Academy of Sciences, Beijing 100049, China;*
[3] *State Key Laboratory of Lithospheric Evolution, Institute of Geology and Geophysics, Chinese Academy of Sciences, Beijing 100029, China;*
[4] *Nu Instruments, Wrexham LL13 9XS, UK;*
[5] *Isotope Laboratory, Department of Earth and Space Sciences, University of Washington, Seattle, WA 98195, USA;*
[6] *Institute of Earth Sciences, China University of Geosciences (Beijing), Beijing 100083, China*

Received March 23, 2022; revised May 4, 2022; accepted May 9, 2022; published online June 20, 2022

Abstract This study presents high-precision analyses of stable potassium (K) isotope ratio using the recently-developed, collision-cell multi-collector inductively coupled plasma mass spectrometry (CC-MC-ICP-MS, Nu Sapphire). The accuracy of our analyses is confirmed by measuring well-characterized geostandards (including rocks and seawater). Our results are consistent with literature values and a precision of 0.04‰ (2SD) has been achieved based on multiple measurements of BCR-2 geostandard over a six-month period. We also evaluate factors that may lead to artificial isotope fractionations, including the mismatches in K concentration and acid molarity between samples and bracketing standards, as well as potential matrices. As the K adsorption capacity of AGW50-X8 (200–400 mesh) is reduced with an increasing amount of matrix elements, less than 150 μg K was loaded during the column chemistry. To evaluate the potential use of K isotopes as an archive of paleo seawater composition, δ^{41}K values of an international seawater standard (IAPSO), a Mn-nodule (NOD-P-1), and two iron formation standards (FeR-2 and FeR-4) are reported. The δ^{41}K value of IAPSO is consistent with other seawater samples reported previously, further substantiating a homogeneous K isotopic distribution in modern global oceans. The K isotopes in Mn-nodule (NOD-P-1: –0.121±0.013‰) and iron formation samples (FeR-2: –0.538±0.009‰; FeR-4: –0.401±0.008‰) seem to be an effective tracer of their formation genesis and compositional changes of ancient seawater. Our results suggest that high-precision measurements of stable K isotopes can be routinely obtained and open up a large variety of geological applications, such as continental weathering, hydrothermal circulation and alteration of oceanic crust.

Keywords CC-MC-ICP-MS, Potassium isotopes, Geostandards, Sample-standard bracketing method, Low energy path

Citation: Li W, Cui M, Pan Q, Wang J, Gao B, Liu S, Yuan M, Su B, Zhao Y, Teng F Z, Han G. 2022. High-precision potassium isotope analysis using the Nu Sapphire collision cell (CC)-MC-ICP-MS. Science China Earth Sciences, 65(8): 1510–1521, https://doi.org/10.1007/s11430-022-9948-6

1. Introduction

Potassium (K) is a rock-forming element concentrated in the continental crust, where it actively cycles through the soil-plant-hydrosphere system and constitutes a major cation in the ocean (Morgan et al., 2018; Tuller-Ross et al., 2019; Hu et al., 2020, 2021a; Huang et al., 2020; Teng et al., 2020). Biologically, it serves as a critical electrolyte in cellular structures (Wang and Wu, 2017; Li et al., 2021a). Potassium has two stable isotopes: ^{39}K (93.258%) and ^{41}K (6.730%), and a minor radioactive isotope ^{40}K (0.012%) that decays to ^{40}Ar and ^{40}Ca. The wide distribution of K motivated studies

* Corresponding authors (email: lwj@mail.iggcas.ac.cn)
† Corresponding authors (email: subenxun@mail.iggcas.ac.cn)

 This work was supported by the Experimental Technology Innovation

of the $^{41}K/^{39}K$ ratio (reported as $\delta^{41}K$) to constrain a diversity of geological and biological processes (see Wang et al., 2021a, for a recent review).

The development of K isotope geochemistry is greatly benefited from the advent of multi-collector inductively coupled plasma mass spectrometer (MC-ICP-MS), which provides significantly improved precision than thermal ionization mass spectrometry (TIMS, e.g., Verbeek and Schreiner, 1967) or secondary ionization mass spectrometry (SIMS, e.g., Humayun and Clayton, 1995a, 1995b). The major challenge for K isotope analysis is the large interferences related to $^{40}Ar^+$ and argon hydrides ($^{38}ArH^+$ and $^{40}ArH^+$) produced by the Ar ICP. Initial attempts have been made by Wang and Jacobsen (2016a) and Li et al. (2016) on single-focusing MC-ICP-MS equipped with a collision/reaction cell that can be used to remove Ar-related interferences. They obtained a typical 2SD (standard deviation) of 0.17 to 0.30‰, and by increasing the number of analyses for a given sample, a 2SE (standard error) of ~0.05‰ can be obtained. A better 2SD (≤0.10‰) has been achieved using double-focusing MC-ICP-MS, and the Ar interferences can be partially resolved using pseudo-high-resolution. This is currently the most widely used method for K isotope analyses (Hu et al., 2018; Morgan et al., 2018; Chen et al., 2019; Li et al., 2020).

With the recent development of high-precision analyses, significant K isotope fractionations have been documented during chemical weathering based on both field studies (Chen et al., 2020; Teng et al., 2020; Li et al., 2021a) and experimental studies (Li et al., 2021b). These processes result in a heterogeneous upper continental crust (Li et al., 2019b; Huang et al., 2020), as well as sediments and surface runoff delivered to the ocean (Hu et al., 2020; Li et al., 2019a, 2022b; Wang et al., 2021b, 2022). The homogeneous K isotopic composition of modern seawater (Hille et al., 2019; Wang et al., 2020) reflects a balance between inputs from rivers and mid-ocean ridge hydrothermal fluids and outputs to seafloor alteration and sediment diagenesis (Parendo et al., 2017; Santiago Ramos et al., 2018, 2020; Hu et al., 2020; Liu et al., 2020). The K isotopic evolution of seawater over geologic timescales may thus provide insights into continental weathering and long-term climate.

Previous studies have mainly focused on low-temperature fractionations because these fractionations are larger and crustal lithologies have higher K contents. Recent studies reveal the great potential of K isotopes as a tracer of high-temperature processes, such as mantle metasomatism (Ionov and Wang, 2021), crustal recycling in arc and intra-plate magmatism (Sun et al., 2020; Hu et al., 2021a; Liu et al., 2021; Parendo et al., 2022; Wang et al., 2021c, 2022), and planetary formation (e.g., Wang and Jacobsen, 2016b; Nie et al., 2021; Tian et al., 2021). In addition, there is a growing interest in studies of K cycling in plants and animal organs using K isotopes (Li, 2017; Christensen et al., 2018; Moynier et al., 2021a), and the development of marine carbonate $\delta^{41}K$ as a paleoenvironmental proxy (Li et al., 2021c, 2022a). These studies typically focus on samples containing much less K, which is challenging using conventional MC-ICP-MS. Although hot plasma has been used to mitigate the sensitivity loss due to the use of high-resolution mode (Chen et al., 2020; Hobin et al., 2021; An et al., 2022), a significantly increased sensitivity (>1000 V ppm^{-1}, 1 ppm=1×10^{-6} g g^{-1}) has been achieved by the latest generation, collision cell-equipped MC-ICP-MS, i.e., the Nu Sapphire (Chen et al., 2021; Moynier et al., 2021b). The Nu Sapphire is characterized by a high-energy ion path (6 kV acceleration), which is a traditional MC-ICP-MS and a low-energy ion path (4 kV acceleration) which contains a collision cell. The hexapole collision cell utilizes He and H_2 gas to remove various Ar-based polyatomic species such as the large $^{40}Ar^+$, together with $^{38}ArH^+$ and $^{40}ArH^+$, which directly interfere with the $^{39}K^+$ and $^{41}K^+$ isotopes (Figure 1). In this way, Ar-based species are almost completely removed, hence K isotopic ratios can be measured in the low-resolution mode.

Here, we evaluate the performance of stable K isotopic analyses of the first Nu Sapphire instrument (SP015) installed in China, following the practice of Moynier et al. (2021b). We achieve a precision of 0.04‰ (2SD) over a six-month period. Our analytical accuracy is confirmed by consistent results obtained for a range of geostandards reported in previous studies. Additionally, we provide high-precision $\delta^{41}K$ value for an international certified seawater standard (IAPSO, International Association for the Physical Sciences of Oceans), further substantiating the K isotopic homogeneity of the global oceans. To assess the potential of using $\delta^{41}K$ as an archive of paleo seawater, we carried out pilot analyses of one Mn nodule standard (NOD-P-1) and two iron formation standards (FeR-2 and FeR-4), which were precipitated from modern and Archean seawater, respectively (Bekker et al., 2010; Koschinsky et al., 2018). Their distinguishable $\delta^{41}K$ values may be related to sedimentary environment and geochemical composition, and further allow inter-laboratory data comparison.

2. Experimental

Sample dissolution and chemical purification for geostandards and seawater were conducted at Metallogenic Elements and Isotopes Lab in the Institute of Geology and Geophysics, Chinese Academy of Sciences (IGGCAS), along with four samples processed at the University of Washington (UW), Seattle (U.S.A.), following established procedures at the University of Washington (UW), Seattle (U.S.A.) (Xu et al., 2019).

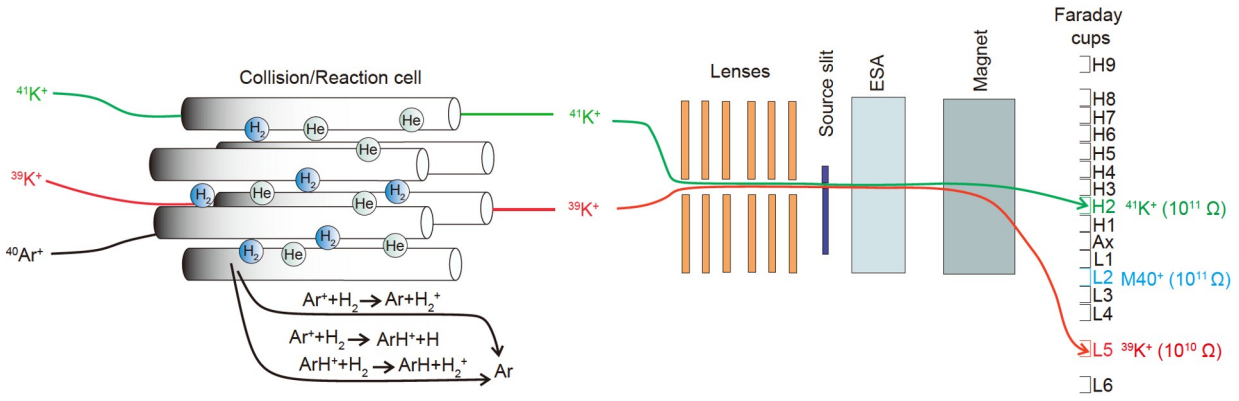

Figure 1 Simplified illustration of the low-energy path of the Nu Sapphire instrument where a collision cell is used to analyze K stable isotopes by removing Ar-based interferences. ESA is short for Electrostatic Analyzer. The plot is not to scale.

2.1 Reagents and materials

High-purity chemical reagents and clean labware were used to maintain low K blanks, including concentrated ultra-pure nitric acid (HNO_3), hydrochloric acid (HCl), and hydrofluoric acid (HF) (CMOS grade, Shanghai Institute of Chemical Reagents), as well as Milli-Q deionized water (resistivity: 18.2 MΩ cm^{-1}) (Elix-Millipore, U.S.A). Teflon beakers (ODLAB, South Korea and Savillax, U.S.A) used for sample digestion and solution collection were cleaned by sequential cleaning using Milli-Q water, 6 mol L^{-1} HCl, and 6 mol L^{-1} HNO_3 at 120°C for a minimum 24 hours for each cycle, and finally rinsed three times with Milli-Q water. All centrifuge tubes, Bio-Rad polyethylene columns (size of 2 mL bed volume (0.8×4 cm) and 10 mL reservoir volume), and pipette tips were cleaned in a 2% (v/v) HNO_3 and ultrapure water for 12 hours on a hot plate at 80°C, then further cleaned with Milli-Q water for three times. The Bio-Rad AG50W-X8 resin (200–400 mesh, H^+ form) was pre-cleaned alternately with CMOS grade 6 mol L^{-1} HCl and Milli-Q water for three times followed by 1 mol L^{-1} HNO_3 and Milli-Q water.

A representative set of geological rocks with diverse chemical compositions were processed and analyzed in this study to verify the accuracy and reproducibility of our K isotopic analyses. These include BCR-2 basalt, AGV-2 andesite, GSP-2 granodiorite, G-2 granite, QLO-1 Quartz latite, NOD-P-1 Mn-nodule from the United States Geological Survey (USGS), two iron formation geostandards FeR-2 and FeR-4 from Canadian Certified Reference Materials Project (CCRMP), and GBW07103 Granite, from Chinese National Research Center for Geoanalysis (CNRCG). We also analyzed four geostandards that were processed and analyzed previously at UW to check the inter-laboratory consistency of the measurements. These samples are JB-1 basalt, from the Geological Society of Japan (GSJ), BHVO-1 basalt, BCR-1 basalt, and G-2 granite from the USGS. A 10,000 ppm K standard solution SRM 3141a purchased from the National Institute of Standards and Technology (NIST) was used as the bracketing standard. Single elemental standard solutions including K, Ca, V, Cr, Rb, Na, Mn, Fe and Al (all 1000 mg L^{-1}) were purchased from the National Research Center for Certified Reference Material, Beijing, China, and diluted in 2% HNO_3 for conditional experiments.

2.2 Sample digestion

Chemical procedure was undertaken in a class-1000 ultra-clean laboratory equipped with class-100 laminar flow exhaust hoods to minimize contamination. Approximately 5–15 mg of sample powders were weighed and digested in pre-cleaned 7 mL Teflon beakers using mixture of 1 mL concentrated HNO_3 and 0.5 mL concentrated HF. For seawater and sedimentary rock samples, 0.5 mL H_2O_2 (CMOS grade, Shanghai Institute of Chemical Reagents) was added to oxidize organics. The beakers were tightly capped and then heated at 150°C on a hot plate for 1–2 days. The digested sample solutions were then evaporated to dryness at 120°C. Samples were then treated with aqua regia (1.5 mL concentrated HCl and 0.5 mL concentrated HNO_3) and heated at 120°C overnight until no precipitation was observed. After evaporation of the solutions to dryness on the hot plate (120°C), the residues were refluxed in 6 mol L^{-1} HNO_3 and dried again after complete digestion. The final residues were fully dissolved in 0.5 mol L^{-1} HNO_3 twice prior to column separation.

2.3 Column separation

The chemical purification process of K followed the method detailed in Xu et al. (2019). The 2 mL pre-cleaned resin was packed into pre-cleaned Bio-Rad column and cleaned with 10 mL Mill-Q H_2O, 10 mL 6 mol L^{-1} HNO_3, and 10 mL Milli-Q H_2O. After conditioning with 10 mL 0.5 mol L^{-1} HNO_3, 1 mL sample solution was loaded into the resin and then eluted with a 15 mL of 0.5 mol L^{-1} HNO_3 to remove the

matrix elements (Ti, Rb, Mg, Fe, Ca, Al and Na). The K fraction containing ~100% of total K was collected with 20 mL 0.5 mol L^{-1} HNO_3. The collected K solution was dried on a hot plate at 100°C and the same purification process was performed again to ensure complete matrix removal. The final solution was dried down and diluted to desired concentration in 2% HNO_3 ready for K isotope ratio determination.

2.4 Mass spectrometry

Potassium isotopic measurements were conducted on the Nu Sapphire CC-MC-ICP-MS (Nu Instruments, Wrexham, UK) in IGGCAS using the low-energy path. An auto-sampler SC-2DX (Elemental Scientific, U.S.A.) was connected to an Apex Omega desolvation nebulizer (Elemental Scientific, U.S.A.) system for sample introduction. Faraday cups L5 and H2 were used in static mode to collect the $^{39}K^+$ and $^{41}K^+$ beams, respectively, and the L2 cup was used to monitor mass 40. The L5 cup was connected to a pre-amplifier fitted with a 10^{10} Ω resistor for the collection of the large $^{39}K^+$ ion beam, while the other two Faraday cups were both connected to pre-amplifiers fitted with conventional 10^{11} Ω resistors (Figure 1).

The preamplifier gain of individual Faraday cup was calibrated prior to K isotopic measurements on a daily basis. A purified K solution (200 ppb yielding ca. 200 V ^{39}K, 1 ppb=1×10^{-9} g g^{-1}) was introduced using a 100 μL min^{-1} self-aspirating nebulizer into the instrument fitted with standard dry Ni cones. Flow rates of the nebulizer gas, Ar sweep gas and other instrumental parameters were optimized prior to the analytical sequence. Each analysis consisted of 1 block of 50 cycles with 4 s integrations. A 60 s blank measurement was conducted in clean 2% HNO_3 every 10 samples. Five to seven repeated analyses were conducted on each sample solution. A bracketing standard solution of SRM 3141a in 2% HNO_3 was prepared for each sample to correct the instrumental isotope fractionation. An 80 s wash in 2% HNO_3 following each measurement plus a transfer time of 70 s before added up to an average of 90 min instrument time per sample (7 repeat measurements). The operating parameters of the instrument are listed in Table S1 online (https://link.springer.com).

The use of a collision cell, in combination with the desolvating nebulizer system for K isotopic measurements, allows measurements of samples with low K concentration at ppb level, which is an order of magnitude lower than those measured on traditional MC-ICP-MS without a collision cell. We obtain a typical ^{39}K sensitivity >1000 V ppm^{-1}. In comparison, the blank of 2% HNO_3 on the masses 39 and 41 were approximatively 1.5 V and 70 mV, respectively, corresponding to the concentration of 1.5 ppb K for the 2% HNO_3 solution. Therefore, the blank contribution to a sample solution containing 150 ppb K is less than 1%. The total procedure blank, including sample digestion, column chemistry, and dilution by 10 mL 2% HNO_3 has a signal of 2.8 V on mass 39 and 170 mV on mass 41, equivalent to 28 ng K, which is negligible compared with tens of μg of K in the solution from sample chemical purification.

3. Results and discussion

Potassium isotopic data are reported in δ notation relative to SRM 3141a, using the sample-standard bracketing technique for instrumental mass fractionation correction:

$$\delta^{41}K(‰) = \left[\frac{(^{41}K/^{39}K)_{sample}}{(^{41}K/^{39}K)_{standard}} - 1\right] \times 1000.$$

The analytical uncertainties are expressed as 2SD and 95% confidence interval (c.i.) (Hu et al., 2018) for five to seven repeat analyses on each sample. The data are reported in Table S2 online and illustrated in Figure 2.

3.1 Analytical accuracy and precision

3.1.1 Analytical precision

To evaluated instrument stability, a series of SRM 3141a solution were measured at varying concentrations, with $\delta^{41}K$ calculated relative to itself. These measurements yield consistent $\delta^{41}K$ values within 2SD uncertainty for the 50 ppb solution ($\delta^{41}K$=–0.013±0.043‰), the 100 ppb solution ($\delta^{41}K$=–0.008±0.025‰), and the 200 ppb solution ($\delta^{41}K$= –0.003±0.026‰). A K concentration of 200 ppb is preferred for sample measurements to reduce the contribution from the procedure blank.

The precision was assessed by 14 measurements of the USGS basalt standard BCR-2 over a period of six months, including 9 separate dissolutions and chemical purifications (Figure 3). We obtained an average $\delta^{41}K$ of –0.423±0.040‰ (2SD, n=14), which is consistent with the literature value (Xu et al., 2019) obtained on conventional MC-ICP-MS and recent results obtained on the Nu Sapphire (Chen et al., 2021; Moynier et al., 2021b). The 2SD of 0.040‰ is taken to represent the intermediate precision for our K isotopic measurements, which compares well with the precision reported for other Nu Sapphire instruments (Ku and Jacobsen, 2020; Chen et al., 2021; Moynier et al., 2021b). In general, the Nu Sapphire CC-MC-ICP-MS offers better external reproducibility than conventional MC-ICP-MS that measures the $^{41}K/^{39}K$ ratio on peak shoulder with cold plasma. For example, a random variation of 0.2‰ in $\delta^{41}K$ has been observed for repeat analyses of BHVO-2 on a Neptune Plus using dry plasma introduction (Chen et al., 2019), and a similar external reproducibility of 0.17‰ is reported using wet plasma introduction (Morgan et al., 2018). The use of low-resolution

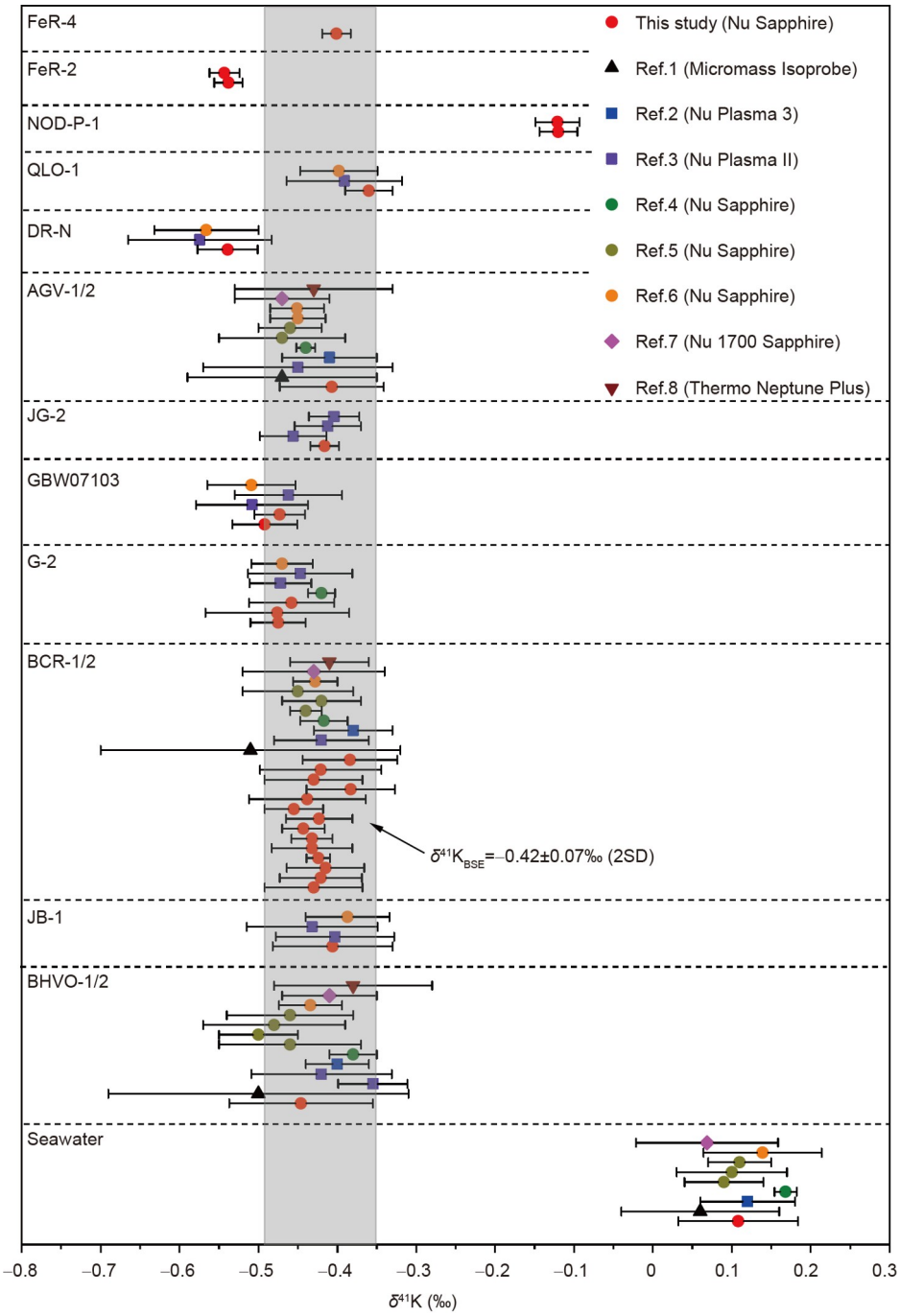

Figure 2 Comparison of δ^{41}K values of selected geological reference materials measured in this study and literature. Shaded area is bulk silicate earth (BSE) value of −0.42±0.07‰ (2SD) from Hu et al. (2021b). Ref.1=Li et al. (2016) by hot plasma via collision cell on single focusing instrument; Ref.2=Li et al. (2020) by cold plasma method; Ref.3=Xu et al. (2019) by cold plasma method; Ref.4=Ku and Jacobsen (2020) by hot plasma via collision cell; Ref.5=Chen et al. (2021) by hot plasma via collision cell; Ref. 6=Moynier et al. (2021b) by hot plasma via collision cell; Ref.7=An et al. (2022) by hot plasma in high resolution; Ref.8=Gu and Sun (2021) by cold plasma in low-resolution. Precision is plotted as 2SD for comparison.

with a collision cell also gives better external precision than measurements made in low-resolution without a collision cell (Gu and Sun, 2021).

3.1.2 Evaluation of analytical accuracy

The accuracy of our analyses is confirmed by measuring geostandards and seawater (Figure 2). Four of these samples were previously analyzed at the UW. They yield identical δ^{41}K values to those measured on a Nu Plasma II at UW (Xu et al., 2019), suggesting measurements made on the Nu sapphire are highly consistent with those made on conventional MC-ICP-MS. The δ^{41}K values of igneous rock standards chemically processed at IGGCAS also agree well with published data reported from various instruments and che-

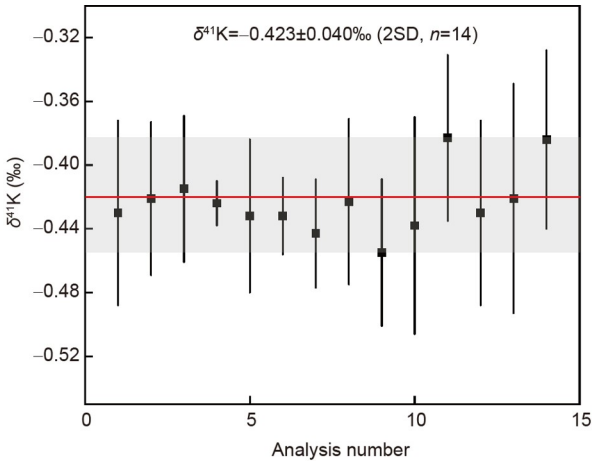

Figure 3 Evaluation of external precision (2SD) of δ^{41}K by 14 analyses over six months for geostandard BCR-2. Error bars are 2SD uncertainties and grey area represents the precision of this study.

mical separations (Xu et al., 2019; Ku and Jacobsen, 2020; Chen et al., 2021; Moynier et al., 2021b), confirming the accuracy of our full procedure, including sample dissolution, column chemistry, and instrumental analysis. We also report δ^{41}K values of geostandards Mn-nodule (NOD-P-1=−0.121±0.013‰) and iron formation (FeR-2=–0.538±0.009‰; FeR-4=–0.401±0.008‰) for the first time.

Seawater provides a secondary in-house standard for accuracy check, and the global oceans represent the most ^{41}K-enriched major terrestrial reservoir. Although a consistent difference in δ^{41}K has been reported between the bulk silicate Earth (BSE) and seawater, the K isotopic composition of individual seawater analyses varies by ~0.2‰ (Li et al., 2016; Morgan et al., 2018; Hille et al., 2019; Wang et al., 2020). Furthermore, the international seawater standard IAPSO has only been measured by Li et al. (2016) and An et al. (2022) using a single-focusing CC-MC-ICP-MS. The δ^{41}K values are reported as 0.06±0.10‰ (Li et al., 2016) and 0.07±0.09‰ (An et al., 2022), respectively. Our analyses of the IAPSO yield a δ^{41}K value of 0.108±0.076‰ (2SD), which is consistent with the average value of the global oceans at 0.12±0.08‰ (2SD) (Hille et al., 2019; Wang et al., 2020) (Figure 4a). Therefore, our analyses further substantiate the K isotopic homogeneity of global oceans, which reflects the long residence time of K in the ocean.

The accumulated high-precision analyses of seawater clearly established that global oceans have a positive δ^{41}K value, which is approximately 0.1‰ higher than the average of –0.01±0.17‰ reported previously in Morgan et al. (2018) as an internal standard for data normalization (Figure 4b). The BSE value reported in Morgan et al. (2018) is also 0.1‰ lower than more recent estimates (e.g., Tuller-Ross et al., 2019; Hu et al., 2021b), which is consistent with the offset of their seawater value relative to global average proposed by Hille et al. (2019) and Wang et al. (2020). We recommend reporting δ^{41}K values relative to the bracketing standard instead of a terrestrial reservoir, because the average K isotopic composition of such a reservoir could be changed with improved precision and accuracy offered by advanced analytical technology.

3.2 Potassium isotopic compositions of Mn-nodule and iron formation

Mn nodules are Mn and Fe oxide segregations precipitated from ambient seawater via hydrothermal, hydrogenous or diagenetic processes (Dymond et al., 1984; Cronan, 2001). The Mn nodule geostandard sample NOD-P-1 was collected from the Pacific Ocean (14°50′00″N, 124°28′00″W) at a depth of 4340 m (Flanagan and Gottfried, 1980). It is believed to be diagenetic based on its Ni+Cu value of 2.6% (Glasby, 2006). The δ^{41}K value (−0.121±0.013‰) of NOD-P-1 obtained in this study is higher than that of BSE (–0.42‰; Hu et al., 2021b) but lower than that of seawater (~0.12‰; Figure 4a). Compared to hydrothermal Mn-nodule from Pacific Ocean (δ^{41}K=−0.02±0.04‰, 95% c.i.; Hu et al., 2020), NOD-P-1 is isotopically lighter K, implying that K isotopic compositions of Mn-nodules may arise from their different origins. Future studies on K isotopes of Mn-nodules will lead to a better understanding of Mn-nodule genesis and tracing compositional changes of ancient seawater.

We also analyzed two Algoma-type iron formation standards FeR-2 sampled from Griffith Mine, Bruce Lake, Canada and FeR-4 from Sherman Mine, Temagami, Canada, both deposited from Archaean ocean (~2.7 Ga). The K isotopic composition of FeR-4 (δ^{41}K=−0.401±0.008‰) is consistent with BSE value within analytical uncertainty, while FeR-2 is isotopically lighter with δ^{41}K of −0.538±0.009‰. The isotopic difference between the two iron formation samples might be relevant to their different mineral assemblage (e.g., amphibole is present in FeR-2 but absent in FeR-4) or variable degrees of metamorphism. This, anyway, indicates that K isotope systematics has application potentials in iron formation genesis and thus deserves further investigation.

3.3 Resin exchange capacity

The total exchange capacity is defined as the maximum theoretical quantity of ions that the resin can load. The K exchange capacity of AG50W-X8 resin involving different concentration of matrix elements was tested by loading the prepared solution onto the column. Three solutions were prepared to contain (1) 50 μg of K plus 50 μg of each matrix element (Na, Mg, Al, Ca, Ti, Fe and Mn), (2) 180 μg of K and 180 μg of each matrix element, and (3) 180 μg of K plus 350 μg of each matrix element. Following the column se-

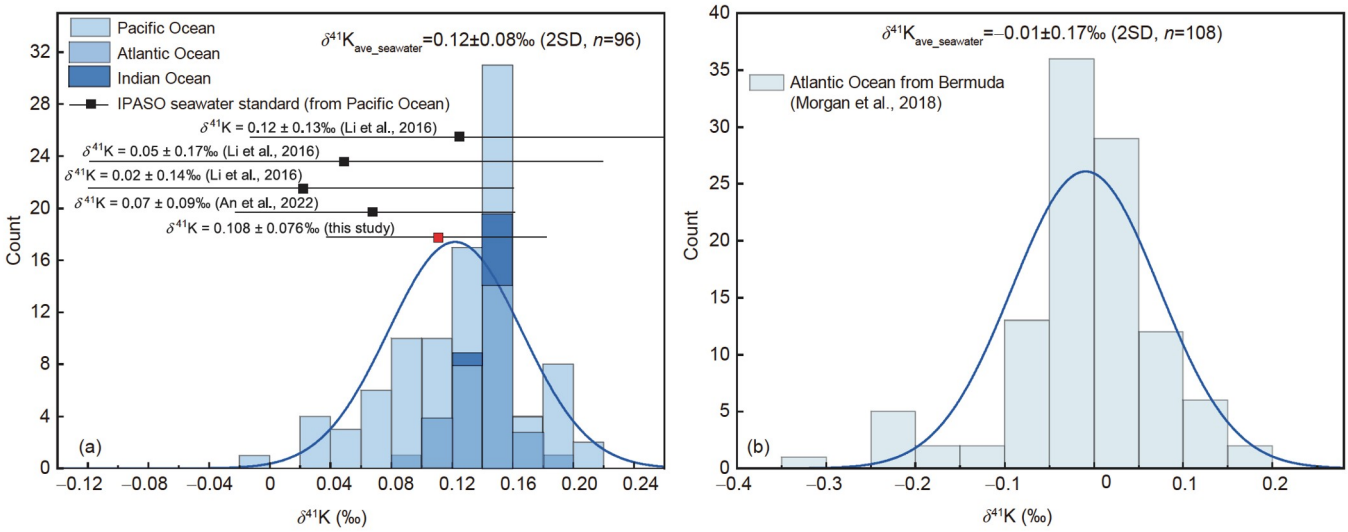

Figure 4 Frequency distribution of δ^{41}K values in global seawater. (a) The seawater data including Pacific Ocean, Atlantic Ocean, and Indian Ocean from Wang et al. (2020) and Hille et al. (2019), as well as five IPASO data yields an average global seawater δ^{41}K value of 0.12±0.08‰. (b) The Bermuda seawater data from Morgan et al. (2018) have an average δ^{41}K value of –0.01±0.17‰.

paration procedure, different fractions of the solution were collected in four steps including matrix elution in 15 mL 0.5 mol L^{-1} HNO_3, K collection in 20 mL 0.5 mol L^{-1} HNO_3, and resin washing by 10 mL 6 mol L^{-1} HCl and 10 mL H_2O after the sample loading. The content of major elements was checked by ICP-OES.

The test result of low K content (50 μg) plus low matrix elements (50 μg×7=350 μg) shows that K collected in 20 mL 0.5 mol L^{-1} HNO_3 was completely separated from the matrix elements with 100% K recovery (Figure 5). For K plus medium matrix elements (180 μg×7=1260 μg), the recovery of K decreased to 96.7%, equivalent to 174 μg K, with 2.4 μg K detected in 10 mL 6 mol L^{-1} HCl. For 180 μg K plus high matrix elements (350 μg×7=2450 μg), the recovery of K was only 95% whereas 171 μg K was recovered from the K cut. Therefore, the exchange capacity of 2 mL wet resin is approximately 170 μg K. Considering more matrix elements existed in natural samples have the further potential to decrease the K exchange capacity, we recommend the amount of K used for column separation to be less than 150 μg for geological samples. It is beneficial to calculate the maximum weight of sample loading on the resin, especially for the high K samples. On the other hand, low K samples are susceptible to high matrix load and more detailed analytical work is required.

In the test of high matrix elements solution, both Al and Na appeared in the K fraction from column separation for the first time (Figure 2). It is therefore recommended that the purification process is conducted twice to ensure complete matrix removal. Also, we have noticed that 25% Fe remained in the resin after matrix washing by 10 mL 6 mol L^{-1} HCl and 10 mL H_2O. We thus recommend changing resin frequently.

3.4 Conditional experiments

Analytical artifacts can be resulted from the mismatch of acid molarity and K concentration between samples and bracketing standards as well as presence of matrix elements. The extents of these effects vary with sample introduction systems, MC-ICP-MS instruments, and settings (Ku and Jacobsen, 2020; Chen et al., 2021; Moynier et al., 2021b; An et al., 2022). In the following sections, we evaluate each of these factors on the Nu Sapphire hosted at IGGCAS.

3.4.1 Effect of HNO_3 concentration

Standard-sample bracketing measurements were carried out with samples diluted in HNO_3 of a range of concentrations from 1% to 5% and standards in 2% HNO_3. Both sample solutions and standard solutions were prepared to have 200 ppb NIST SRM 3141a K solution. The δ^{41}K exhibits a strong negative correlation with acid molarities with R^2=0.96 (Figure 6). For example, a 3% difference in acid molarity between the sample and the standard would result in a negative offset of 1.05‰ in δ^{41}K. These effects are consistent with the results reported on the Sapphire instrument by Chen et al. (2021) but differ from another Sapphire instrument that documented a positive correlation between acid molarity and δ^{41}K (Moynier et al., 2021b). Thus, using the same batch of 2% HNO_3 for both sample and standard dilution is critical to obtaining accurate results.

3.4.2 Effect of K concentration

Previous studies revealed that concentration mismatch between samples and standards can have a strong effect on δ^{41}K (Chen et al., 2019, 2021; Moynier et al., 2021b; An et al., 2022). To assess the tolerance for K concentration mismatch

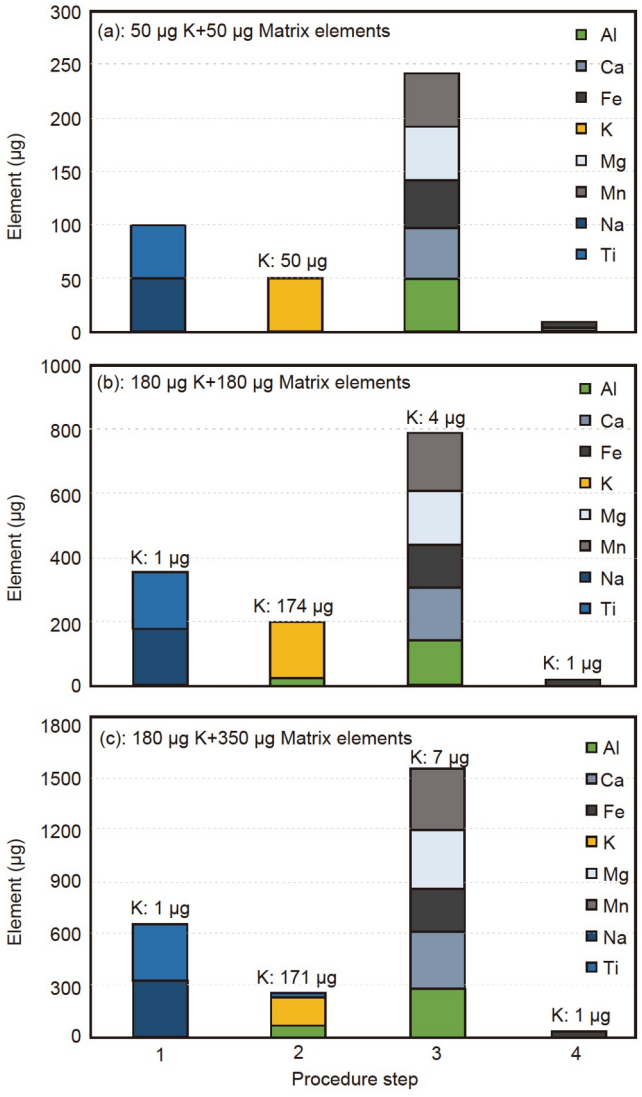

Figure 5 Plots of elution bar for various combinations of K content and doping matrix elements (Al, Ca, Fe, K, Mg, Mn, Na, and Ti) contents in selected column separation procedure steps. The first step includes sample loading and matrix elution by 15 mL 0.5 mol L^{-1} HNO_3. The second step is 20 mL 0.5 mol L^{-1} HNO_3 for K collection. The third step is 10 mL 6 mol L^{-1} HCl for resin cleaning. The last step is the 10 mL H_2O for resin cleaning again.

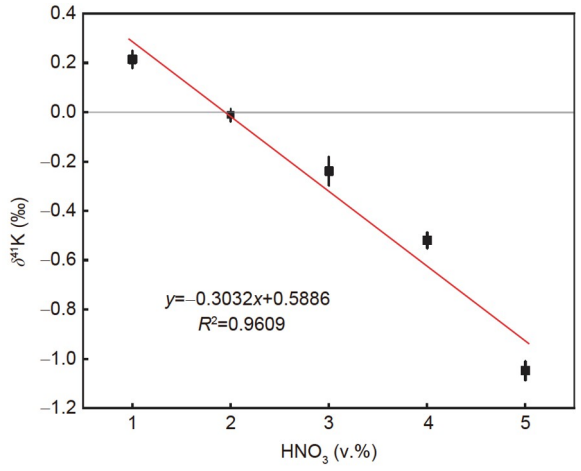

Figure 6 Effect of HNO_3 molarity mismatch between sample and standard on $\delta^{41}K$ value. Sample used here is 200 ppb SRM 3141a K solution dissolved in HNO_3 at molarities ranging from 1% to 5%. All measurements were bracketed by a 200 ppb SRM 3141a solution in 2% HNO_3. Each $\delta^{41}K$ data point represents average value of five replicate analyses, and error bars are 2SD uncertainties.

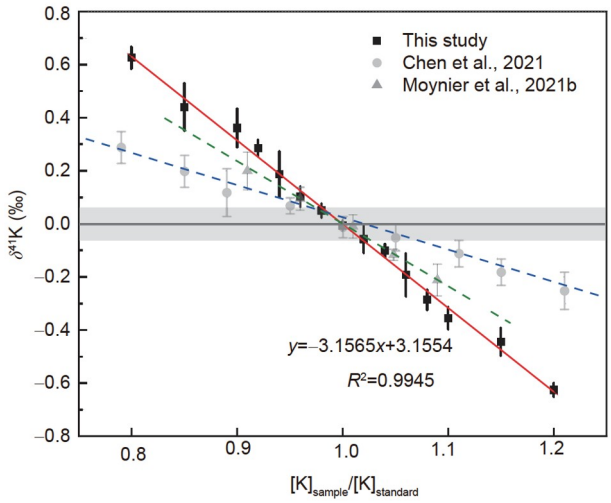

Figure 7 Effect of K concentration mismatch between sample and standard on $\delta^{41}K$ value. $[K]_{sample}/[K]_{standard}$ represents K concentration ratio between sample and standard. All measurements were bracketed by a 200 ppb pure K solution. Data from Chen et al. (2021) and Moynier et al. (2021b) are also plotted for comparison. Each $\delta^{41}K$ data point represents average value of seven replicate analyses, and error bars are 2SD uncertainties.

K sample solutions were prepared at various concentrations and were measured against a 200 ppb bracketing standard, with sample/standard concentration ratio varying from 0.7 to 1.3.

We first observe a negative correlation between measured offset in $\delta^{41}K$ and intensity mismatch, with ~0.05‰ isotopic bias at 2% mismatch (Figure 7). This agrees with the results reported by Chen et al. (2021) and Moynier et al. (2021b). However, to a larger concentration mismatch scale (up to 20%), it is observed the $\delta^{41}K$ value offsets are various from different Sapphire instruments (Figure 7). Taking into account of our precision of 0.04‰, we recommend an intensity match within 2% between the sample and bracketing standard for obtaining accurate $\delta^{41}K$ data.

We further optimized instrumental tuning parameters to achieve a higher tolerance for K concentration mismatch. Very stable $^{41}K/^{39}K$ measurements with a high internal precision (SE of 5.78×10^{-7}) were observed whilst the ^{39}K intensity went up from 182 V to 193 V during a single analysis (Figure 8). This indicated that a 5% ^{39}K intensity mismatch may not lead to any offset in $\delta^{41}K$. We then performed the concentration test using the SRM 3141a solution and a geostandard (BCR-2) with 0–30% K intensity mismatch against the SRM 3141a standard. The results show that ac-

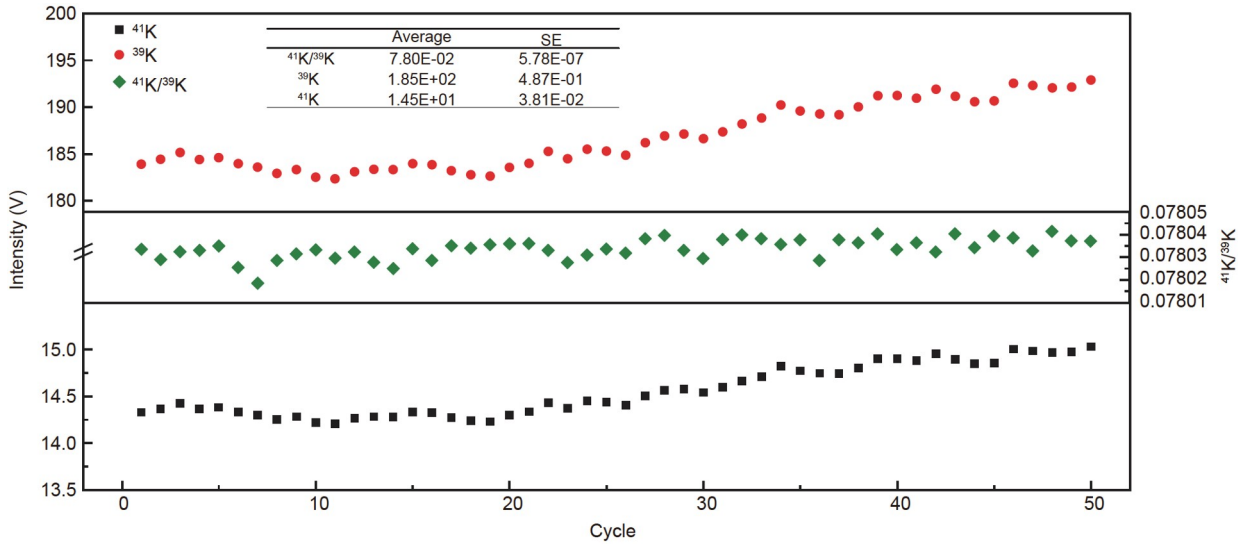

Figure 8 Intensities of ^{39}K and ^{41}K as well as $^{41}K/^{39}K$ ratio of the 200 ppb K solution over 50 cycles in a single analysis.

curate and precise K isotopic results can be obtained at concentration mismatch within 20% (Figure 9), which is consistent with the 14% intensity mismatch tolerance reported by Ku and Jacobsen (2020). This effect is likely related to tuning parameters matching between the desolvation nebulizer system and instrument setting. The extended range of concentration mismatch tolerance from 1–2% to 20% allows much easier access to highly precise and accurate K isotopic measurements.

3.4.3 *Matrix effect*

Although column chemistry can remove most of the matrix elements, there remain some matrix elements that may be retained in purified K solutions. These matrix elements can form polyatomic species that interfere directly with K isotopes, e.g., $^{23}Na^{16}O^{+}$ on $^{39}K^{+}$, $^{25}Mg^{16}O^{+}$, $^{23}Na^{18}O^{+}$ and $^{40}Ca^{1}H^{+}$ on $^{41}K^{+}$, as well as induce instrumental mass bias. Here we tested the impact of Mg, Na, Ca, V, Cr, Rb, and Ca on the accuracy of K isotopic measurements. All tests were performed with 200 ppb K solution, e.g., which 1% Mg corresponds to 2 ppb of Mg, and the matrix element-doped K solutions were then measured against pure K solution. Since elution interval of K overlaps largely with that of Rb and Cr on cation exchange resin (e.g., Chen et al., 2019; Xu et al., 2019), the influence of Rb on K isotope analysis was examined by deliberately doping the pure K solutions with Rb to obtain a wide range of [Rb]/[K] concentration ratio from 0.1 to 1.0. Although the other elements can be completely separated from K, they are potential contaminants from the laboratory environment. These elements (Mg, Na, Ca, V, Cr and Ca) are doped to 1%, 2%, 4% or 5%, and 10% of the K.

The test results illustrated in Figure 10 suggest that Ca causes the largest matrix effects of all elements. Mg and Rb, when less than 10% of the K, have negligible influence on

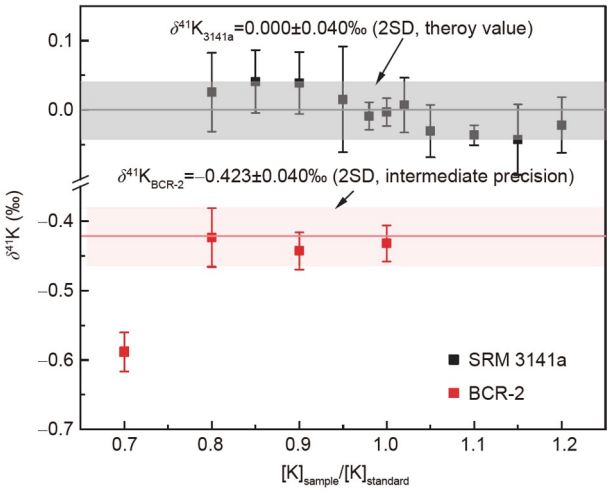

Figure 9 Re-evaluated effect of K concentration mismatch on $\delta^{41}K$ value. $[K]_{sample}/[K]_{standard}$ ratio represents K concentration ratio of SRM 3141a and BCR-2 solution against SRM 3141a standard. Error bars are 2SD uncertainties.

the $\delta^{41}K$ value. Na, V and Cr all induce a negative shift of the $\delta^{41}K$, therefore their concentrations should be limited to within 2% of the K. The presence of Ca is particularly problematic for K analysis as it can cause a significant shift of $\delta^{41}K$ to higher values, e.g., a Ca/K ratio of 1% (~2 V of ^{40}Ca in our case, equivalent to 2 ppb of Ca) would lead to a +0.065‰ elevation in $\delta^{41}K$. Our results are comparable to two other Sapphire analyses on similar matrix doping tests (Chen et al., 2021; Moynier et al., 2021b). Taking into account the analytical uncertainty, the Ca/K ratio of the solution should not exceed 1%, in other words, the Ca concentration should not be higher than 2 ppb in a 200 ppb K solution. If more than 1% Ca and 2% other matrix elements remain in the solution, additional chemical separation will be

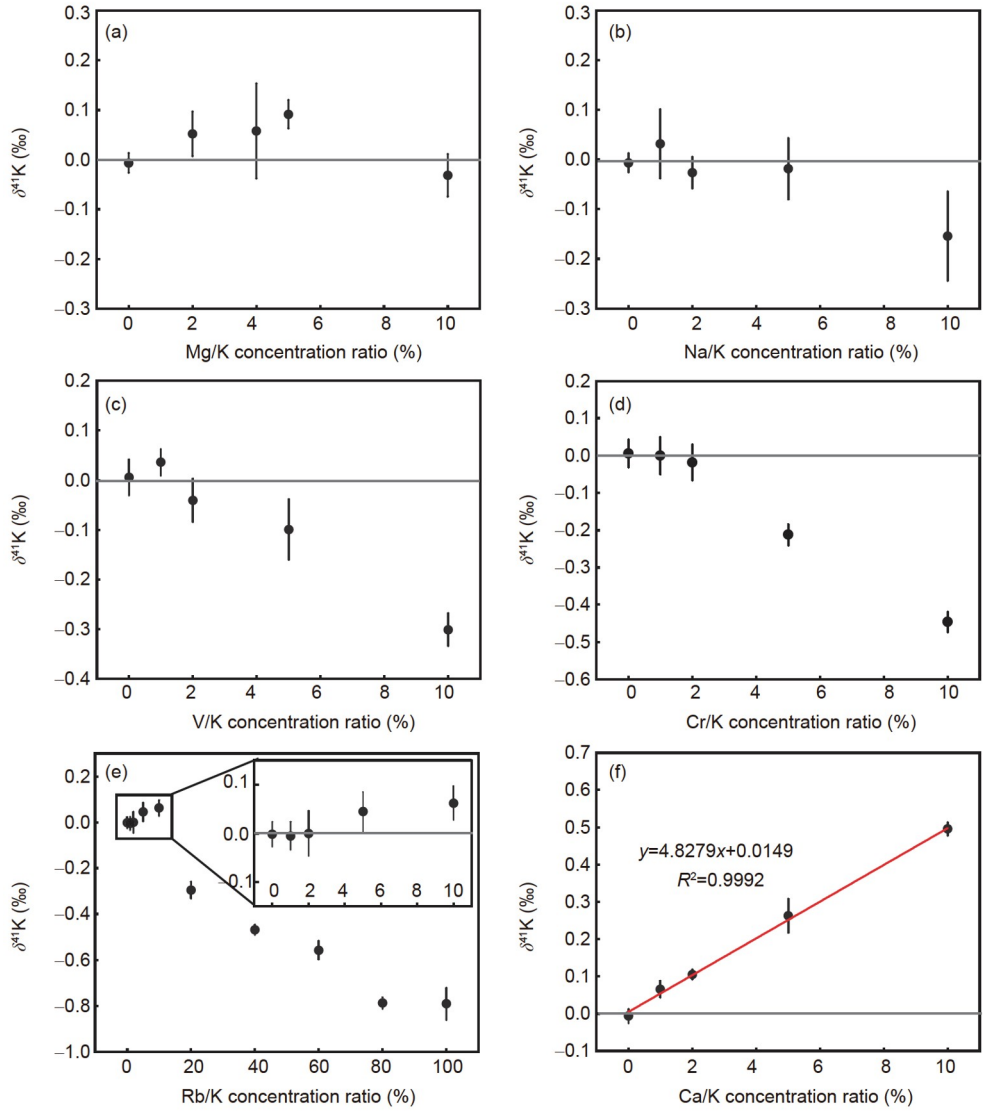

Figure 10 Effect of matrix elements of (a) Mg, (b) Na, (c) V, (d) Cr, (e) Rb, and (f) Ca on K isotopic measurements. Each δ^{41}K data point represents average value of five replicate analyses, and error bars are 2SD uncertainties.

required. It should be noted that the effect reported above is related to the instrument setting and desolvating nebulizer system parameters utilized in our study.

4. Conclusions

This study describes the analytical method of K isotopic analysis employing the collision cell technique on the Nu Sapphire instrument. Compared to high resolution- and cold plasma (RF=~700 W) methods applied on traditional MC-ICP-MS, collision cell and hot plasma (RF=1300 W) result in much higher instrument sensitivity of ca. 1000 V ppm^{-1} for ^{39}K. We evaluate the possible effects of K concentration mismatch, and mismatch of acid molarity as well as matrix elements on the accuracy of sample-standard bracketing measurements. The optimized measurement conditions include: (1) using less than 150 μg K content from samples to perform column separation; (2) dilution of sample and standard using 2% HNO_3 from the same batch; (3) matching of sample and standard K concentrations up to within 20%; (4) controlling Ca concentration to below 1% relative to the K concentration in the purified sample solution; (5) Limiting other matrix elements such as Na, Mg, Rb, Cr and V concentration to below 2% relative to the K concentration. Following these measurement conditions, the accuracy and precision of our analyses have been validated by measuring both pure standards and well-characterized geostandards. Our results agree well with previously reported values within analytical uncertainties, with a precision (over six months) of ±0.04‰ (2SD). It demonstrates that this method provides an efficient way to precisely determine K isotopes. The newly

obtained K isotopic values of Mn-nodule and BIF geostandards are likely related to their sedimentary environment, yet, more related studies are required to investigate behavior of K isotopes in modern/paleo oceans.

Acknowledgements *We would like to thank Qinghan YUAN, Xuyang ZHENG, and Xiaoqiang LI for the development of K isotope analysis and Yanhong LIU for assistance in ICP-OES analysis. We also thank Yan HU, Zidong PENG, the anonymous reviewers and the editor-in-Chief Yongfei ZHENG for insightful comments and helpful discussions. This study was financially supported by the Experimental Technology Innovation Fund of the Institute of Geology and Geophysics, Chinese Academy of Sciences (Grant No. TEC 202103) and the Youth Innovation Promotion Association, Chinese Academy of Sciences.*

References

An S, Luo X, Li W. 2022. Precise measurement of $^{41}K/^{39}K$ ratios by high-resolution multicollector inductively coupled plasma mass spectrometry under a dry and hot plasma setting. Rapid Comm Mass Spectrometry, 36: e9289

Bekker A, Slack J F, Planavsky N, Krapez B, Hofmann A, Konhauser K O, Rouxel O J. 2010. Iron formation: The sedimentary product of a complex interplay among mantle, tectonic, oceanic, and biospheric processes. Economic Geol, 105: 467–508

Chen H, Liu X M, Wang K. 2020. Potassium isotope fractionation during chemical weathering of basalts. Earth Planet Sci Lett, 539: 116192

Chen H, Saunders N J, Jerram M, Halliday A N. 2021. High-precision potassium isotopic measurements by collision cell equipped MC-ICPMS. Chem Geol, 578: 120281

Chen H, Tian Z, Tuller-Ross B, Korotev R L, Wang K. 2019. High-precision potassium isotopic analysis by MC-ICP-MS: An inter-laboratory comparison and refined K atomic weight. J Anal At Spectrom, 34: 160–171

Christensen J N, Qin L, Brown S T, DePaolo D J. 2018. Potassium and calcium isotopic fractionation by plants (soybean [*glycine max*], rice [*oryza sativa*], and wheat [*triticum aestivum*]). ACS Earth Space Chem, 2: 745–752

Cronan D S. 2001. Manganese nodules. In: Steele J H, ed. Encyclopedia of Ocean Sciences, Second edition. Oxford: Academic Press. 488–495

Dymond J, Lyle M, Finney B, Piper D Z, Murphy K, Conard R, Pisias N. 1984. Ferromanganese nodules from MANOP Sites H, S, and R—Control of mineralogical and chemical composition by multiple accretionary processes. Geochim Cosmochim Acta, 48: 931–949

Flanagan F J, Gottfried D. 1980. USGS rock standards; III, Manganese-nodule reference samples USGS-Nod-A-1 and USGS-Nod-P-1. 1155

Glasby G. 2006. Manganese: Predominant role of nodules and crusts. In: Schulz H D, Zabel M, eds. Marine Geochemistry. Springer, Berlin, Heidelberg. 371–427

Gu H O, Sun H. 2021. High-precision analysis of potassium isotopes by MC-ICP-MS without collision cell using cool plasma technique in low-resolution mode. J Anal At Spectrom, 36: 2545–2552

Hille M, Hu Y, Huang T Y, Teng F Z. 2019. Homogeneous and heavy potassium isotopic composition of global oceans. Sci Bull, 64: 1740–1742

Hobin K, Costas Rodríguez M, Vanhaecke F. 2021. Robust potassium isotopic analysis of geological and biological samples via multicollector ICP-Mass spectrometry using the "extra-high resolution mode". Anal Chem, 93: 8881–8888

Hu Y, Chen X Y, Xu Y K, Teng F Z. 2018. High-precision analysis of potassium isotopes by HR-MC-ICPMS. Chem Geol, 493: 100–108

Hu Y, Teng F Z, Plank T, Chauvel C. 2020. Potassium isotopic heterogeneity in subducting oceanic plates. Sci Adv, 6: eabb2472

Hu Y, Teng F Z, Chauvel C. 2021a. Potassium isotopic evidence for sedimentary input to the mantle source of Lesser Antilles lavas. Geochim Cosmochim Acta, 295: 98–111

Hu Y, Teng F Z, Helz R T, Chauvel C. 2021b. Potassium isotope fractionation during magmatic differentiation and the composition of the mantle. J Geophys Res-Solid Earth, 126: e2020JB021543

Huang T Y, Teng F Z, Rudnick R L, Chen X Y, Hu Y, Liu Y S, Wu F Y. 2020. Heterogeneous potassium isotopic composition of the upper continental crust. Geochim Cosmochim Acta, 278: 122–136

Humayun M, Clayton R N. 1995a. Potassium isotope cosmochemistry: Genetic implications of volatile element depletion. Geochim Cosmochim Acta, 59: 2131–2148

Humayun M, Clayton R N. 1995b. Precise determination of the isotopic composition of potassium: Application to terrestrial rocks and lunar soils. Geochim Cosmochim Acta, 59: 2115–2130

Ionov D A, Wang K. 2021. Potassium distribution and isotope composition in the lithospheric mantle in relation to global Earth's reservoirs. Geochim Cosmochim Acta, 309: 151–170

Jiang Y, Koefoed P, Pravdivtseva O, Chen H, Li C H, Huang F, Qin L P, Liu J, Wang K. 2021. Early solar system aqueous activity: K isotope evidence from Allende. Meteorit Planet Sci, 56: 61–76

Koschinsky A, Heinrich L, Boehnke K, Cohrs J C, Markus T, Shani M, Singh P, Smith Stegen K, Werner W. 2018. Deep-sea mining: Interdisciplinary research on potential environmental, legal, economic, and societal implications. Integr Environ Assess Manag, 14: 672–691

Ku Y, Jacobsen S B. 2020. Potassium isotope anomalies in meteorites inherited from the protosolar molecular cloud. Sci Adv, 6: eabd0511

Li S, Li W, Beard B L, Raymo M E, Wang X, Chen Y, Chen J. 2019a. K isotopes as a tracer for continental weathering and geological K cycling. Proc Natl Acad Sci USA, 116: 8740–8745

Li W. 2017. Vital effects of K isotope fractionation in organisms: Observations and a hypothesis. Acta Geochim, 36: 374–378

Li W, Beard B L, Li S. 2016. Precise measurement of stable potassium isotope ratios using a single focusing collision cell multi-collector ICP-MS. J Anal At Spectrom, 31: 1023–1029

Li W, Li S, Beard B L. 2019b. Geological cycling of potassium and the K isotopic response: Insights from loess and shales. Acta Geochim, 38: 508–516

Li W, Liu X M, Hu Y, Teng F Z, Hu Y F, Chadwick O A. 2021a. Potassium isotopic fractionation in a humid and an arid soil-plant system in Hawai'i. Geoderma, 400: 115219

Li W, Liu X M, Hu Y, Teng F Z, Hu Y. 2021b. Potassium isotopic fractionation during clay adsorption. Geochim Cosmochim Acta, 304: 160–177

Li W, Liu X M, Wang K, Fodrie F J, Yoshimura T, Hu Y F. 2021c. Potassium phases and isotopic composition in modern marine biogenic carbonates. Geochim Cosmochim Acta, 304: 364–380

Li W, Liu X M, Wang K, Hu Y, Suzuki A, Yoshimura T. 2022a. Potassium incorporation and isotope fractionation in cultured scleractinian corals. Earth Planet Sci Lett, 581: 117393

Li X, Han G, Liu M, Liu J, Zhang Q, Qu R. 2022b. Potassium and its isotope behaviour during chemical weathering in a tropical catchment affected by evaporite dissolution. Geochim Cosmochim Acta, 316: 105–121

Li X, Han G, Zhang Q, Miao Z. 2020. An optimal separation method for high-precision K isotope analysis by using MC-ICP-MS with a dummy bucket. J Anal At Spectrom, 35: 1330–1339

Liu H, Wang K, Sun W D, Xiao Y, Xue Y Y, Tuller-Ross B. 2020. Extremely light K in subducted low-T altered oceanic crust: Implications for K recycling in subduction zone. Geochim Cosmochim Acta, 277: 206–223

Liu H Y, Xue Y Y, Wang K., Sun W D, Wang K. 2021. Contributions of slab-derived fluids to ultrapotassic rocks indicated by K isotopes. Lithos, 396-397: 106202

Morgan L E, Santiago Ramos D P, Davidheiser-Kroll B, Faithfull J, Lloyd N S, Ellam R M, Higgins J A. 2018. High-precision $^{41}K/^{39}K$ measurements by MC-ICP-MS indicate terrestrial variability of $\delta^{41}K$. J Anal At Spectrom, 33: 175–186

Moynier F, Hu Y, Dai W, Kubik E, Mahan B, Moureau J. 2021a. Potassium isotopic composition of seven widely available biological standards using collision cell (CC)-MC-ICP-MS. J Anal At Spectrom, 36: 2444–2448

Moynier F, Hu Y, Wang K, Zhao Y, Gérard Y, Deng Z, Moureau J, Li W, Simon J I, Teng F Z. 2021b. Potassium isotopic composition of various samples using a dual-path collision cell-capable multiple-collector inductively coupled plasma mass spectrometer, Nu instruments Sapphire. Chem Geol, 571: 120144

Nie N X, Chen X Y, Hopp T, Hu J Y, Zhang Z J, Teng F Z, Shahar A, Dauphas N. 2021. Imprint of chondrule formation on the K and Rb isotopic compositions of carbonaceous meteorites. Sci Adv, 7: eabl3929

Parendo C A, Jacobsen S B, Wang K. 2017. K isotopes as a tracer of seafloor hydrothermal alteration. Proc Natl Acad Sci USA, 114: 1827–1831

Parendo C A, Jacobsen S B, Kimura J I, Taylor R N. 2022. Across-arc variations in K-isotope ratios in lavas of the Izu arc: Evidence for progressive depletion of the slab in K and similarly mobile elements. Earth Planet Sci Lett, 578: 117291

Santiago Ramos D P, Coogan L A, Murphy J G, Higgins J A. 2020. Low-temperature oceanic crust alteration and the isotopic budgets of potassium and magnesium in seawater. Earth Planet Sci Lett, 541: 116290

Santiago Ramos D P, Morgan L E, Lloyd N S, Higgins J A. 2018. Reverse weathering in marine sediments and the geochemical cycle of potassium in seawater: Insights from the K isotopic composition ($^{41}K/^{39}K$) of deep-sea pore-fluids. Geochim Cosmochim Acta, 236: 99–120

Sun Y, Teng F Z, Hu Y, Chen X Y, Pang K N. 2020. Tracing subducted oceanic slabs in the mantle by using potassium isotopes. Geochim Cosmochim Acta, 278: 353–360

Teng F Z, Hu Y, Ma J L, Wei G J, Rudnick R L. 2020. Potassium isotope fractionation during continental weathering and implications for global K isotopic balance. Geochim Cosmochim Acta, 278: 261–271

Tian Z, Magna T, Day J M D, Mezger K, Scherer E E, Lodders K, Hin R C, Koefoed P, Bloom H, Wang K. 2021. Potassium isotope composition of Mars reveals a mechanism of planetary volatile retention. Proc Natl Acad Sci USA, 118: e2101155118

Tuller-Ross B, Savage P S, Chen H, Wang K. 2019. Potassium isotope fractionation during magmatic differentiation of basalt to rhyolite. Chem Geol, 525: 37–45

Verbeek A A, Schreiner G D L. 1967. Variations in ^{39}K:^{41}K ratio and movement of potassium in a granite-amphibolite contact region. Geochim Cosmochim Acta, 31: 2125–2133

Wang K, Jacobsen S B. 2016a. An estimate of the Bulk Silicate Earth potassium isotopic composition based on MC-ICPMS measurements of basalts. Geochim Cosmochim Acta, 178: 223–232

Wang K, Jacobsen S B. 2016b. Potassium isotopic evidence for a high-energy giant impact origin of the Moon. Nature, 538: 487–490

Wang K, Close H G, Tuller-Ross B, Chen H. 2020. Global average potassium isotope composition of modern seawater. ACS Earth Space Chem, 4: 1010–1017

Wang K, Li W, Li S, Tian Z, Koefoed P, Zheng X Y. 2021a. Geochemistry and cosmochemistry of potassium stable isotopes. Geochemistry, 81: 125786

Wang K, Peucker-Ehrenbrink B, Chen H, Lee H, Hasenmueller E A. 2021b. Dissolved potassium isotopic composition of major world rivers. Geochim Cosmochim Acta, 294: 145–159

Wang Y, Wu W H. 2017. Regulation of potassium transport and signaling in plants. Curr Opin Plant Biol, 39: 123–128

Wang Z Z, Teng F Z., Prelević D, Liu S A, Zhao Z. 2021c. Potassium isotope evidence for sediment recycling into the orogenic lithospheric mantle. Geochem Persp Let, 18: 43–47

Wang Z Z, Teng F Z, Busigny V, Liu S A. 2022. Evidence from HP/UHP metasediments for recycling of isotopically heterogeneous potassium into the mantle. Am Miner, 107: 350–356

Xu Y K, Hu Y, Chen X Y, Huang T Y, Sletten R S, Zhu D, Teng F Z. 2019. Potassium isotopic compositions of international geological reference materials. Chem Geol, 513: 101–107

(Responsible editor: Yongfei ZHENG)